To cite this version :

Local Measurements for the Study of External Loop Airlift Hydrodynamics

MARIANNE UTIGER[1], FRANK STUBER[2†], ANNE-MARIE DUQUENNE[2*], HENRI DELMAS[2] and CHRISTOPHE GUY[1]

[1] *Département de génie chimique, École Polytechnique de Montréal, C. P. 6079, Succursale Centre-Ville, Montréal, QC H3C 3A7, Canada*

[2] *École Nationale Supérieure d'Ingénieurs de Génie Chimique (ENSIGC), 18 Chemin de la Loge, 31078 Toulouse Cedex 4, France*

Hot-film anemometry and an optical biprobe are used to measure local flow characteristics in the riser of an external loop airlift reactor. Important flow asymmetries are observed above the sparger and developing flow persists through a large part of the riser. As gas flow rate increases, radial gas hold-up profiles change from relatively flat to parabolic while the shape of radial liquid velocity profiles remains constant and Sauter bubble diameter increases. At large gas superficial velocities, slip velocity is found to deviate considerably from the frequently used value of 0.25 m/s. Local measurements allow a better understanding of two-phase flow in airlift reactors and can be used for CFD-modeling development and validation.

L'anémométrie à film chaud et une bisonde optique ont servi à caractériser l'hydrodynamique locale de la zone ascendante d'un airlift à boucle externe. Des asymétries importantes de l'écoulement sont observées au-dessus du distributeur et l'écoulement se développe dans une grande partie du riser. Avec l'augmentation du débit de gaz, les profils radiaux de taux de vide passent de relativement plats à paraboliques tandis que la forme des profils de vitesse du liquide demeure constante et que le diamètre de Sauter des bulles augmente. Aux grands débits de gaz, la vitesse de glissement est considérablement différente de 0.25 m/s, valeur classiquement utilisée. Les mesures locales permettent une meilleure compréhension de l'écoulement diphasique en réacteur airlift et peuvent être utilisées pour le développement et la validation de modèles de mécanique des fluides numériques.

Keywords: airlift reactors, hydrodynamics, local measurements, two-phase flow.

Airlift reactors have become increasingly popular in the past two decades. They can be used for a wide range of applications, such as bioprocesses, waste water treatment and, in the chemical industry, for hydrogenation and oxidation of organic products. Of simple construction, these reactors provide good phase contact for mass transfer and require a relatively low energy input. Also, compared to bubble columns, they can be operated at higher gas throughputs and achieve better mixing and wall heat transfer. However, proper design and scale-up of airlift reactors remain difficult due to the complex hydrodynamics of the gas–liquid flow.

Numerous studies are reported in the literature. In general, global variables are used to describe airlift hydrodynamics. Riser and downcomer gas hold-up, as well as mean liquid velocity, have been measured in reactors of various geometries. Many empirical correlations have been proposed, but due to the strong influence of reactor geometry on hydrodynamics, their application is often limited to the reactor studied. In fact, downcomer to riser cross section area ratio (Chisti, 1989), reactor height (Russell et al., 1993; Bentifraouine et al., 1997), gas–liquid separator configuration (Siegel and Merchuk, 1991), size of passage area in the bottom section (Merchuk et al., 1994) and sparger type and location (Becker et al., 1994), all affect flow characteristics considerably.

Numerous models, mostly based on a momentum or energy balance, have also been developed. To predict mean liquid velocity, these models generally include a friction factor or friction coefficients, and sometimes require the knowledge of gas hold-up in the riser and downcomer (e.g. Chisti et al., 1988). In other models, slip velocity becomes a second parameter (e.g. Garcia Calvo and Leton, 1996). For the air/water system, a fixed value of 0.25 m/s is often used.

In all cases, the friction factor remains difficult to evaluate, because too little is known on friction in two-phase flows, especially in particular geometric configurations. Experimental friction factors for two-phase flow in airlift reactors are much larger than calculated one-phase factors (Hsu and Dudukovic, 1980; Akita et al., 1988; Young et al., 1991). Correlations for two-phase friction factors given in literature also underestimate frictional effects in airlift reactors (Young et al., 1991). According to Garcia Calvo (1992), the differences observed can originate from the liquid velocity profile. Indeed, the kinetic energy associated with a parabolic liquid velocity profile, such as can be found in the riser of an airlift reactor, can be twice as high as that corresponding to a flat profile. Knowledge of radial velocity profiles in airlift reactors is, therefore, essential.

More recently, models based on more fundamental concepts of fluid mechanics have been developed. Attempts to describe airlift hydrodynamics through multidimensional two-fluid models, based on point continuity and momentum equations for the gas and liquid phase, have been undertaken (Sokolichin and Eigenberger, 1994). This approach, generally referred to as computational fluid dynamics (CFD), is already commercially used for simulation of one-phase flows. CFD modeling has the advantage of taking into account all geometrical parameters which, as mentioned previously, have a strong influence on airlift hydrodynamics. However, for such models to give accurate results, a better quantitative understanding of the local behavior of two-phase flows is required.

Up to now, only a few studies reporting on measurements of both radial and axial variations of hydrodynamic parameters have been conducted. Nicol and Davidson (1988) measured local gas and liquid phase characteristics in an airlift reactor operating in the churn turbulent regime. Another detailed study of an external loop airlift was conducted by Young et al. (1991). Gas and liquid velocities showed strong radial dependency. Becker et al. (1994) measured local velocities of both phases as well as local gas hold-up and bubble size distributions in a flat rectangular loop reactor. Experimental data were compared to CFD simulation results and relatively good agreement was obtained. In a study by Rueffer et al. (1995), local measurements were made in both the air/water system and CMC solutions. Recently, Bentifraouine (1997) also measured local gas phase characteristics in an external loop airlift reactor using water and CMC solutions as the liquid phase.

The objective of this study is twofold. First and foremost, to improve understanding of two-phase flow hydrodynamics in airlift reactors and to show how local measurements can help to achieve this. Secondly, to establish a set of local flow data which can be used to drive CFD modeling efforts and eventually to validate results.

Measurement techniques and signal treatment

Hot-Film Anemometry

Gas hold-up and liquid phase flow characteristics were measured with a constant temperature anemometer (DANTEC 55M01 anemometer with 55M10 standard bridge) equipped with a hot-film probe (DANTEC type 55R11) whose sensitive element is 70 μm in diameter and 1.25 mm in length. Any flow modification which affects heat transfer between the probe and the fluid, and hence changes the probes temperature and resistance, can be detected quasi-instantaneously by the anemometer. Therefore, if fluid temperature and properties remain constant, the voltage of the anemometer signal will be a function of liquid velocity. In the case of two-phase flow, since the gas/probe convective heat transfer coefficient is much smaller than the liquid/probe coefficient, phase change can easily be detected while measuring velocity fluctuations of the continuous phase, when this phase is present at the tip of the probe.

An acquisition frequency of 2 kHz is chosen in order to obtain precise bubble signals, while maximizing measurement precision of liquid flow properties. The number of data points per acquisition is limited to 200 000, resulting in a measuring time of 100 s. In order to link the anemometer voltage to the corresponding liquid velocity, the hot-film probe is calibrated against a Pitot tube in a 50 mm diameter vertical pipe. Distilled water is used; its temperature is regulated to 30.0 ± 0.1°C. For the calibration procedure, an acquisition frequency of 1 kHz and measurement period of 1 min is chosen.

The use of hot-film anemometry in two-phase flow has been reviewed by Bruun (1995). An example of an anemometry signal obtained in an air/water flow is shown in Figure 1. When a bubble passes over the hot-film probe, a sudden fall of the anemometer signal occurs, followed by an abrupt rise when the probe is again immersed in the liquid. Fluctuations are also observed in the liquid phase signal. These represent fluctuations in liquid velocity caused by turbulence. Some other bubble signal characteristics should be
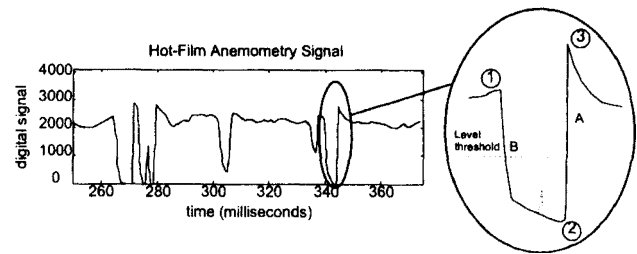

Figure 1 — Anemometer signal obtained in an air/water flow at U_G = 0.046 m/s and signal corresponding to a bubble passage.

mentioned. Bubble-probe contact corresponds to point 1 (Figure 1). A liquid meniscus remains attached to the probe as the bubble continues to rise. On some occasions, this meniscus will rupture during bubble passage, creating a sharp upward peak in the anemometer signal as illustrated in Figure 1. In most cases however, the water film does not break until the arrival of the back of the bubble (point 2). Because liquid in a bubble wake rises faster than the bulk liquid, the anemometer signal immediately after bubble passage is higher than that corresponding to bulk liquid velocity.

Before flow properties can be evaluated, proper signal treatment must be applied to differentiate between signal parts of the gas and liquid phases. For this, points 1, 2 and 3 must be correctly identified for each bubble. The signal treatment program developed, first detects bubbles with the help of a positive slope threshold to find the sharp rise at the end of each bubble signal. From this identified point (point A), one searches forward through the signal to find point 3. In the same way, point 2 is found by searching backward through the signal from point A. From point 2, one then applies a level threshold in order to avoid confusing a possible meniscus breakage peak with the front of the bubble. In this way one finds point B and from there, by searching backward through the signal, point 1. More details on the signal treatment used are given in the work of Utiger (1998).

Once points 1, 2 and 3 have been identified, calculation of gas hold-up, average liquid velocity and velocity fluctuations is straightforward. Bubble passage time corresponds to the interval between points 1 and 2. Gas hold-up is therefore obtained from temporal integration of these signal sections. For the calculation of liquid flow properties, the signal section between points 2 and 3 (Figure 1) must also be eliminated since it is not representative of liquid velocity. The calibration equation is then applied to the remaining anemometry signal.

Optical biprobe

For measurement of local gas phase flow properties, a double optical fiber probe (RTI Instrumentation and Measure) was used, having a known distance of 3.2 mm between the fibers. The diameter of the sensitive optical element is approximately 40 μm. Phase detection is possible due to different refraction indexes of gas and liquid. This measuring technique has been discussed previously by Choi and Lee (1990).

The optical biprobe and its electronic support (opto-electronic module) have a rapid response (in the range of 0.5 to 1 μs), so that local phase changes in gas–liquid flows may be followed quasi instantaneously, even at high bubble frequency. As with hot-film anemometry experiments, an acquisition frequency of 2 kHz was used, allowing measurement
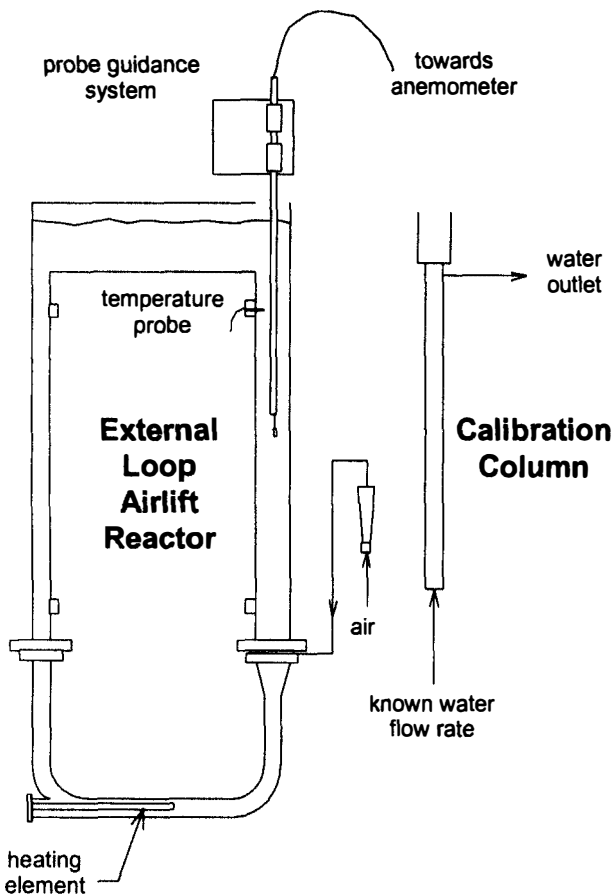
Figure 2 — Experimental set-up.
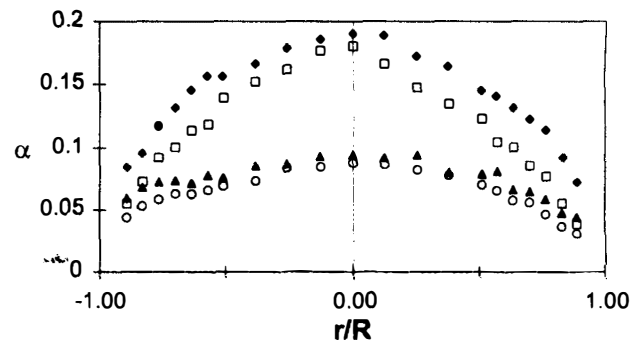
Comparison of Gas Hold-Up Profiles

Figure 3 — Comparison of gas hold-up profiles obtained from the optical biprobe $\blacktriangle$ U_G = 0.029 m/s $\blacklozenge$ U_G = 0.068 m/s and hot-film anemometry $\bigcirc$ U_G = 0.029 m/s $\square$ U_G = 0.068 m/s at axial position z/D = 10.6.

the measured chord lengths, different diameters of interest can be calculated, such as the equivalent diameter d_{10} and the mean Sauter diameter d_{32}, defined as follows:

$$d_{10} = \frac{\sum n_i d_i}{N}, \quad d_{32} = \frac{\sum n_i d_i^3}{\sum n_i d_i^2} \quad \dots \dots \dots \dots \dots (1, 2)$$

Experimental

Measurements were taken in the riser of an external loop airlift reactor 1.79 m in height, made of altuglass (Figure 2). The riser and downcomer have inner diameters of 94 and 50 mm, respectively. The distance between the axis of both columns is 675 mm. The bottom connection is a 50 mm diameter pipe. Elbows are rounded (curvature radius of 125 mm) to reduce pressure drop and prevent dead zones. The 200 mm high head section whose width varies from 94 mm above the riser, to 50 mm above the downcomer, is open to the atmosphere. The gas sparger, located immediately above the enlargement in the riser, 340 mm above the bottom elbow, is formed of 8 parallel tubes pierced with a total of 56 holes, 11 mm apart and 0.6 mm in diameter. In the bottom connection, the airlift reactor is equipped with a heating element to regulate the fluid temperature in the riser to 30.0 ± 0.2°C.

Distilled water was used as the liquid phase in order to avoid anemometer probe fouling. The flow rate of compressed air was regulated with a previously calibrated gas rotameter. A non-aerated liquid height of 1.67 m was used throughout the experiments, resulting in a water volume of 16.5 L. This height was chosen in order to avoid air being sucked into the downcomer. Radial profiles, oriented in the riser-downcomer plane, were obtained at 5 different axial positions in the riser at 0.10, 0.25, 0.50, 0.75 and 1 m above the gas distributor (z/D = 1.0, 2.6, 5.3, 7.9 and 10.6). Superficial gas velocities of 0.029, 0.047 and 0.068 m/s were studied.

Gas hold-up profiles obtained from the optical biprobe and hot-film anemometry compare well (Figure 3), although hot-film anemometry seems to underestimate hold-up slightly. This is probably caused by bubble signals that are incorrectly interpreted as two bubbles instead of one due to large meniscus breakage peaks. The gas and liquid flow rates estimated by surface integration of the local measurements agree well with each other, and with the directly measured values to within an 11% average error.

times of 70 s and the observation of 300 to 3000 bubbles, depending on gas velocity and the location of the probe in the reactor.

For each probe, bubble passage is detected by applying a level threshold to the recorded signal. Gas hold-up is then obtained directly from temporal integration of the gas events recorded by the first probe. Afterwards, by calculating the intercorrelation function of the two signals, the most probable bubble velocity is determined. A range is then defined around this velocity in which, for each bubble passage, a corresponding bubble passage is searched for on the channel corresponding to the second fiber (Roig et al., 1998). For all associated bubbles (bubbles found on both channels) the exact velocity is calculated and the passage time on the first fiber is converted to a corresponding chord length. Chord length classes are then defined and a discrete chord length distribution is obtained. When the gas hold-up is assumed to be locally constant (over one bubble diameter) and the form of the bubble is assumed to be either a sphere or an ellipsoid, the corresponding bubble size distribution can be calculated.

The statistical analysis of our chord length distributions is based on the work of Clark and Turton (1988) for the case of spherical bubbles. The authors predicted the bubble size distribution by backward transformation of the measured chord length distribution. Kamp et al. (1995) extended the analysis to ellipsoidal bubble shapes and developed a software code used in this work. To avoid negative probabilities, as obtained during classical backward transformation, their algorithm includes an approximated log-normal bubble size distribution (as generally observed from experimental bubble size data). Once the bubble size distribution is obtained from

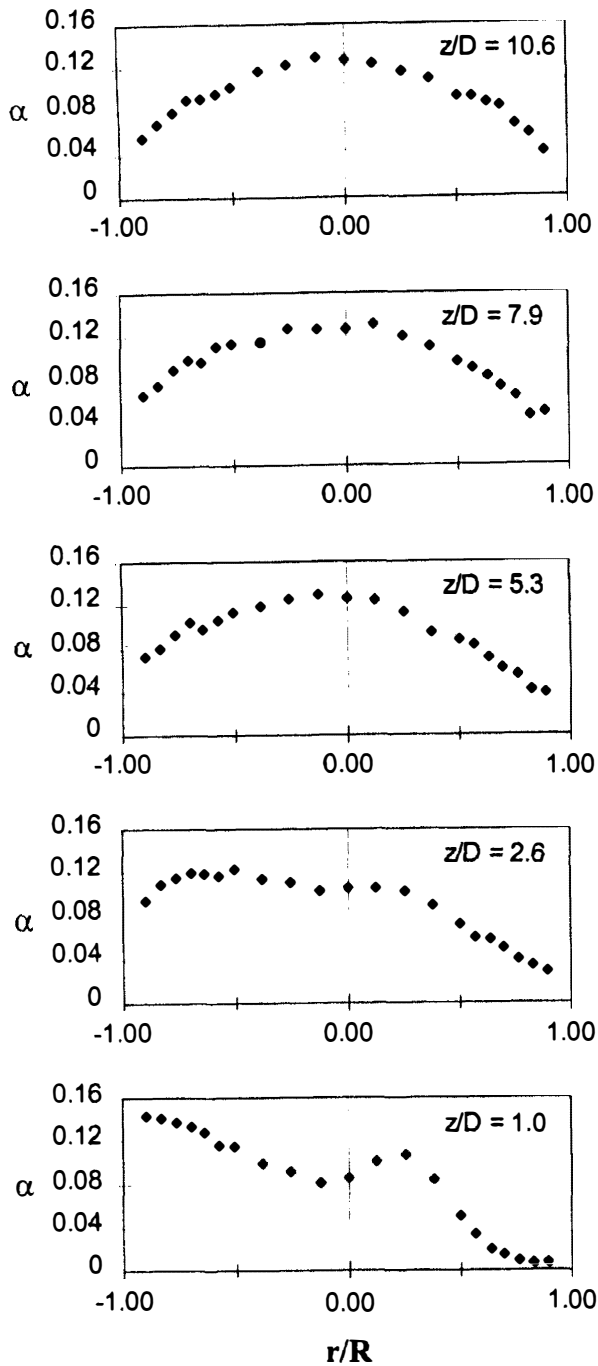# Gas Hold-Up Profiles

Flow profiles at axial position z/D = 7.9

Figure 4 — Gas hold-up profiles (obtained from hot-film anemometry) at different axial positions for gas superficial velocity of 0.047 m/s.

Figure 5 — Flow profiles at axial position z/D = 7.9 ● U_G = 0.029 m/s, □ U_G = 0.047 m/s, ▲ U_G = 0.068 m/s.

Results and discussion

For all flow properties measured, strong asymmetries can be observed in the bottom section of the riser, particularly at higher gas flow rates. Radial profiles become more uniform as the flow moves axially upwards, indicating developing gas–liquid flow (Figure 4). Such developing flow and asymmetric profiles have been previously observed in airlift reactors (Chisti, 1989; Young et al., 1991; Becker et al., 1994; Bentifraouine, 1997). Therefore, only radial profiles in the well developed flow found in the top section of the airlift will be discussed.

GAS HOLD-UP, VELOCITIES AND BUBBLE SIZE

Gas hold-up

Gas hold-up increases with gas flow rate from approximately 5.5 to 9.5% for the three flow rates studied. As can be seen in Figure 5, gas hold-up profiles are relatively flat at the lower superficial velocity, and become more and more parabolic as gas flow increases. Hold-up near the wall remains almost unchanged, while it increases considerably in the center (local maximal values of 9, 13 and 17%). In fact, an increase in flow rate implies the presence of a larger
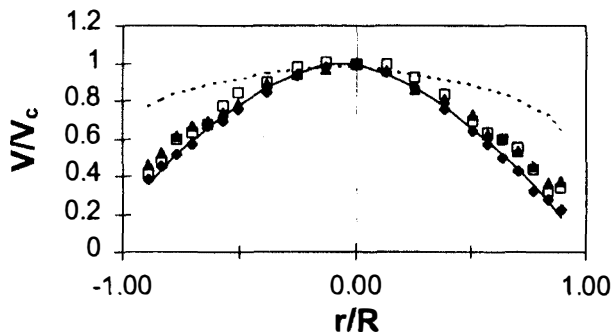
Figure 6 — Normalized velocity profiles and curve fit at position $z/D = 7.9$: ◆ $U_G = 0.029$ m/s, ☐ $U_G = 0.047$ m/s, ▲ $U_G = 0.068$ m/s, --- 1/7 power law profile, —— curve fit, $n = 1.69$.

number of bubbles which favors coalescence and the production of larger bubbles. These bubbles have a tendency to go towards the center of the column (Liu, 1993), thereby increasing gas hold-up in this region. These results are, however, different than those obtained by Young et al. (1991). They found relatively flat hold-up profiles regardless of gas flow rate, although they worked with similar gas superficial velocities, observed similar bubble sizes and also used purified water. Small differences in water quality may, nevertheless, be the reason for the observed differences. Nicol and Davidson (1988), who worked at very high gas superficial velocities, obtained even more parabolic profiles, which seems to confirm the tendency observed in this study. However, the shape of their profiles did not change with gas flow rate. This might be explained by a difference in the flow regime (churn turbulent in their case).

Liquid velocity

As for gas hold-up, liquid velocities increase with gas flow rate (see Figure 5). Average values are about 0.20, 0.25 and 0.27 m/s, whereas central maximal velocities are 0.40, 0.47 and 0.53 m/s. Radial profiles of liquid velocity are strongly parabolic but, contrarily to gas hold-up profiles, their shape does not change with gas flow rate. In fact, radial velocity profiles normed by the maximal velocity all fall on the same curve as shown in Figure 6. Young et al. (1991) obtained similar results for their 0.14 m downcomer with a D_d/D_r ratio of 0.73. However, for their smaller downcomer, with a D_d/D_r ratio closer to that of this study (0.47 compared to 0.53), they observed liquid velocity profiles that become more and more parabolic with increasing gas flow rate (trend seen in this work for gas hold-up profiles). Rueffer et al. (1995), observed slightly flatter liquid velocity profiles, probably due to their very small downcomer ($D_d/D_r = 0.33$) which gave rise to much lower mean liquid velocities. Nicol and Davidson (1988) who, as mentioned previously, worked with much higher gas superficial velocities (0.13 to 0.50 m/s) in an airlift with a D_d/D_r ratio of 1, found liquid velocity profiles in the 1/7th power law form, as in one-phase liquid flow. This is clearly not the case in this study (Figure 6), nor is it expected. Since radial gas phase distribution is non-uniform (more gas occurs in the center) and rising bubbles carry liquid behind them in trailing wakes, the local liquid velocity in the center of the column is greater in two-phase flow, than if only single-phase flow occurred. Hence, for identical superficial liquid velocities, the radial velocity profile in gas–liquid two-phase flow will be more parabolic than the profiles in single-phase flow.

Garcia Calvo (1992) suggested the following equation to represent radial liquid velocity profiles:

$$\frac{V_L - \overline{V_L}}{V_{Lc} - \overline{V_L}} = 1 - 2^{n/2}\left(\frac{r}{R}\right)^n \quad \dots \dots \dots \dots \dots \dots (3)$$

which fits data from this study relatively well with a value of $n = 1.69$ (Figure 6). Young et al. (1991) described their flow profiles with the following equation:

$$\frac{j}{j_c} = 1 - \left(\frac{r}{R}\right)^m \quad \dots \dots \dots \dots \dots \dots \dots \dots (4)$$

where j is the superficial mixture velocity. If only their upper more uniform radial profiles are considered, average values of $m = 1.86$ and $m = 2.53$ are obtained for their 140 and 89 mm diameter downcomer, respectively. For comparison, experimental data from this study gives an intermediate average value of $m = 2.19$. The exponents of these two similar equations are therefore, quite different. It should be pointed out, that mixture superficial velocity is not a very practical variable to use for airlift reactors. Although quite useful in vertical two-phase upflow in pipes, j, which is equal to the sum of gas and liquid superficial velocities, is not a value readily available, or even directly measurable in the case of airlift reactors. In addition, liquid velocity profiles, not superficial mixture velocity profiles, are needed to properly evaluate friction energy losses in models based on an energy balance on the airlift loop. For these reasons, the velocity profile proposed by Garcia Calvo (1992) is preferred.

Bubble velocity

Bubble velocities relative to fixed coordinates (as measured by the optical biprobe) are presented in Figure 5. Average values increase with gas flow rate from 0.56 to 0.75 m/s. Profile shape is similar to that of liquid velocity profiles, although it seems slightly flatter, and remains unchanged with an increase in gas flow rate. Axial variations are found to be negligible at positions 0.50 m or more above the gas distributor ($z/D \geq 5.3$), indicating that constant bubble velocity has been reached. As a comparison, Young et al. (1991) also obtained radial bubble velocity profiles with shapes similar to their liquid velocity profiles, and this for both downcomers used.

Relative bubble velocity ($V_G - V_L$) profiles can be computed from gas and liquid velocity data. Radial profiles obtained, reveal much more scatter in data than other flow properties and are therefore, not shown. However, relative velocities increase with gas flow rate, averaging 0.28, 0.31 and 0.37 m/s, respectively, at the three superficial gas velocities studied. This is certainly due to the corresponding increase in bubble population density and bubble diameter. One concludes that slip velocities may differ considerably with the value of 0.25 m/s often used in airlift modeling, especially at high gas flow rates.

Bubble diameters

Bubble Sauter diameters are calculated assuming ellipsoidal bubble shape. It is worth noting that the use of this hypothesis in flow data treatment leads to an increase of 1 to 1.5 mm in the length of the horizontal bubble axis, when

Figure 7 — Comparison of equivalent and Sauter bubble diameters. d_{32}: ◆ $U_G = 0.029$ m/s, ▲ $U_G = 0.068$ m/s; d_{10}: ◇ $U_G = 0.029$ m/s, △ $U_G = 0.068$ m/s.

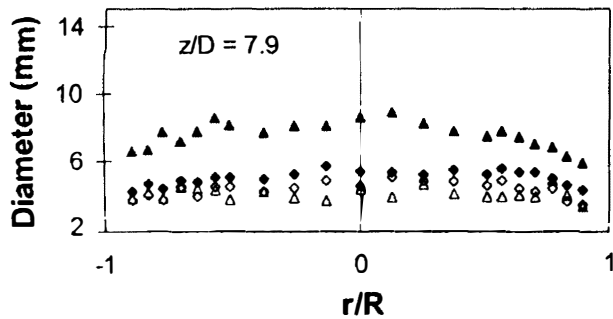Figure 8 — Liquid velocity fluctuations at axial position $z/D = 7.9$ ◆ $U_G = 0.029$ m/s, □ $U_G = 0.047$ m/s, ▲ $U_G = 0.068$ m/s.

compared to spherical bubbles. Independent visual observation of gas bubbles with the aid of a camera confirmed deviation from spherical shape for bubble diameters greater than about 1 to 2 mm.

Radial profiles of bubble Sauter diameter are reported in Figure 5. Average values of 4.9, 6.5 and 7.7 mm are obtained for the three gas flow rates studied. As can be seen, profiles show slight central maxima. Radial variation of the Sauter diameter ranges between 20 and 30% of the maximum values. Axial variation for the three upper measuring positions is of the order of ± 0.2, ± 0.2 and ± 0.5 mm, for gas flow rates of 0.029, 0.047 and 0.068 m/s, respectively. Thus, the axial dependence of the local bubble size, due to the small hydrostatic pressure expansion, appears to be modest with respect to the increase of bubble diameter caused by the change in gas flow rate. Increase in bubble size with gas flow rate was also observed by Nicol and Davidson (1988), who found average bubble Sauter diameters based on spherical shape of about 4 mm.

The higher the gas superficial velocity, the more bubbles are present in the flow, favoring coalescence and the formation of larger bubbles. In turbulent flow, bubble size is however controlled by the equilibrium between dynamic pressure and surface tension forces (Calderbank, 1967). The increase in liquid velocity with gas flow rate should therefore counteract the increase in bubble size due to coalescence. An explanation for this can be found when comparing bubble Sauter diameters (d_{32}) to equivalent diameters (d_{10}). A large difference between these two average diameters will tend to indicate the existence of two bubble populations, or a wide bubble size distribution. In fact, the presence of a few very large bubbles can increase the bubble Sauter diameter considerably, while the equivalent diameter remains relatively unchanged.

Examining profiles at $z/D = 7.9$ (Figure 7), one sees that at the lower superficial gas velocity, d_{32} is only slightly higher than d_{10}, indicating a fairly homogenous bubble population. For the higher gas flow rate however, bubble Sauter diameter is almost 2 mm higher than d_{10}, indicating the presence of large bubbles. In addition, the equivalent diameter seems to diminish with the increase in gas flow rate, such as predicted by the force equilibrium. Although a few large bubbles will affect the bubble Sauter diameter considerably, it still should be used for flow characterization in airlift reactors, since d_{32} is directly related to interfacial area ($a = 6\varepsilon_G/d_{32}$). The presence of very large bubbles, as observed for $U_G = 0.068$ m/s, may indicate transition towards the churn turbulent flow regime. The bimodal distribution evi-
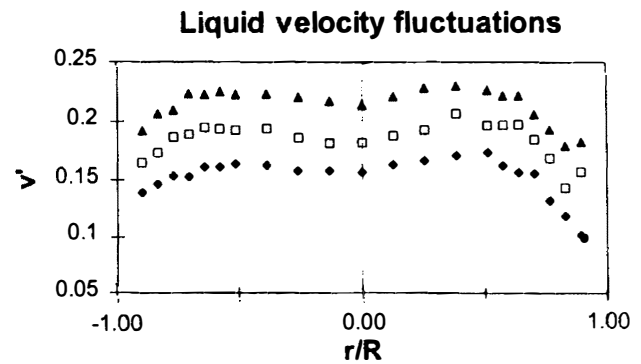
denced in this study is similar to the one observed in bubble columns at and above the transition towards churn turbulent flow (Hyndman et al., 1997).

LIQUID VELOCITY FLUCTUATIONS AND TURBULENCE INTENSITY

Before discussing turbulence related results, a short explanation on the nature of two-phase turbulence is necessary. As mentioned previously, liquid velocity takes into account both the bulk of the liquid phase and the faster rising bubble wakes. Calculated liquid velocity fluctuations are, therefore, composed of both the velocity fluctuations of the bulk liquid and the difference between bulk liquid and wake velocities. The first term can be referred to as intrinsic liquid turbulence, whereas the second term is the bubble induced turbulence, sometimes called pseudo-turbulence. The measured values are of course the sum of both of these terms. In some cases, bubble-induced turbulence has been shown to contribute more than 90% of the total turbulent energy (Liu and Bankoff, 1993).

As with other flow properties, the shape of velocity fluctuation profiles (Figure 8) seems established at positions 0.5 m or more above the sparger. Fluctuations are lower in the center, maximum about half way between the center and the wall, and again lower close to the wall. Such profiles with two maxima have been observed previously in a bubble column (Menzel et al., 1990). On the other hand, in two-phase upflow in vertical pipes, velocity fluctuation profiles go from concave shaped (central minimum) to convex shaped (central maximum), depending on operating conditions (Liu and Bankoff, 1993).

Velocity fluctuations can be related to the local mixing mechanism. Luebbert and Larson (1990) concluded that the prevailing local mixing mechanism in bubble columns and airlift reactors is a combination of diffusional mixing and convective mixing, due to the wakes of rising bubbles. Schmidt et al. (1992) showed that bubble wake associated mixing is less important near the riser wall and in the center of the column. Since there are less bubbles near the riser wall, bubble wake associated mixing is lower in this region. In the center of the column, relative bubble velocities are lower (Schmidt et al., 1992), thus explaining the lesser importance of convective mixing. The velocity fluctuation profiles obtained in this study show the same trend. Velocity fluctuations near the riser wall are lower because less bubbles and hence, less bubble wakes, are found in this region. In the center, relative bubble velocities may well be lower, although computed relative velocity profiles do not permit to conclude this because of too much scatter in the data.
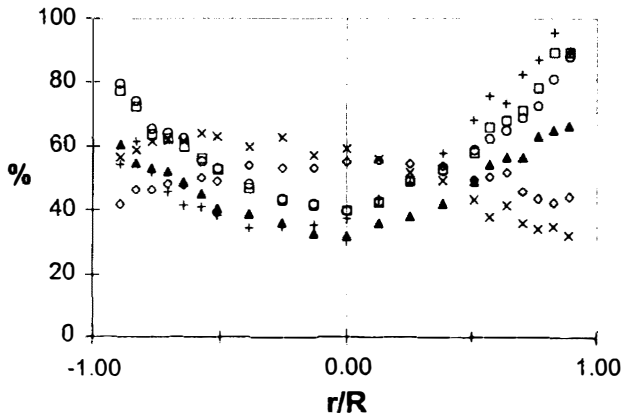
Turbulence intensity and bubble association

Figure 9 — Turbulence intensity (**+** z/D = 2.6, **▲** z/D = 5.3, **☐** z/D = 7.9, **○** z/D = 10.6) and bubble association ratio (**x** z/D = 2.6, **◇** z/D = 7.9) at superficial gas velocity U_G = 0.068 m/s.

Turbulence intensity ($\sqrt{\overline{v_L^2}} / \overline{V_L} = v' / \overline{V_L}$) profiles, shown in Figure 9, have a concave parabolic form. This shape is reported in the literature for both airlift reactors (Young et al., 1991) and two-phase vertical upflow in pipes (Liu and Bankoff, 1993). Central turbulence intensity values at the two highest axial positions are approximately 38% regardless of gas flow rate. Turbulence intensities near the wall can become quite high (more than 80%). However, these results should be considered with caution. Stagnant bubbles (most likely indicating the presence of downflow) could sometimes be observed near the riser wall. Since hot film-anemometry can not distinguish the direction of flow, results in regions of occasionnal downflow are not very reliable.

Although the turbulence intensity profile shape seems established for positions 0.5 m (z/D = 5.3) or more above the sparger, a closer inspection shows that values of both velocity fluctuations and turbulence intensity are much lower at z/D = 5.3 than at z/D = 7.9 and z/D = 10.6. The two latter profiles more or less coincide (Figure 9). This is observed for all gas flow rates studied. It seems that turbulence increases and reaches a constant value at z/D = 7.9, indicating that flow continues to develop up to this position, despite the fact that gas hold-up and velocities are relatively invariant for $z/D \geq 5.3$. Second order flow properties, such as velocity fluctuations and turbulence intensity, may, therefore, be better indicators of developed flow than first order properties, such as velocities and gas hold-up. Developing flow considerations are important since, as shown by experimental data, such flow can prevail in a large portions of the airlift reactor, considerably affecting the energy balance through significantly higher friction factors (Young et al., 1991).

From the optical biprobe signal treatment program, one obtains, among other variables, the bubble association rate, defined as the ratio of the number of bubbles that pass over both probes to the number of bubbles that pass over the first probe. Interestingly, radial bubble association rate profiles have the same shape as turbulence intensity profiles, except upside-down, as can be seen in Figure 9. Hence, bubble association rate is high when turbulence is relatively low, and vice versa. This seems logical since increased turbulence will more often deviate bubbles from the second probe.

Since the bubble association rate and turbulence intensity profile shapes are opposite, but otherwise almost identical, the former may be used to obtain an approximation of the latter when only an optical biprobe is available.

Conclusion

Studies featuring local measurements are still scarce, although such measurements are essential for a better understanding of two-phase flow in airlift reactors. In the reactor studied, developing flow persists through a large portion of the riser. Developing flow will have a much lesser effect on hydrodynamics in a taller unit, which should be kept in mind when considering scale-up. Also, stagnant bubbles indicating local downflow were sometimes observed near the riser wall.

In the upper part of the riser, where flow profile shapes are established, central gas hold-up values increase considerably with gas flow rate, while values near the wall remain almost unchanged. This can be related to the formation of large bubbles that tend to migrate towards the center of the riser, thereby increasing the gas hold-up in this region. At larger gas velocities, two bubble size populations were shown to exist; one of a few very large bubbles and one of many small bubbles. Such a bimodal bubble size distribution has been associated previously with the transition to the churn-turbulent regime.

The shape of liquid velocity profiles does not vary with gas flow rate, and can be represented by an equation suggested by Garcia Calvo (1992). This profile equation can be used in existing models to help evaluate friction energy losses in the riser. At large gas flow rates, where bubble density is high, slip velocity, that also appears in several models, is found to deviate considerably from the frequently used value of 0.25 m/s. Whereas, where liquid velocity fluctuations are concerned, they can be related to the local mixing mechanism. Radial velocity fluctuation profiles indicate that convective mixing due to bubble wakes is most important about half way between the riser wall and the center of the column.

Further work is still necessary to understand two-phase flow in airlift reactors. Studies on two-phase turbulence, as well as bubble rupture and coalescence phenomena, need to be pursued. CFD modeling seems a promising approach, in particular because it can take into account all geometrical parameters. However, such model development and validation cannot be made without local experimental data. The experimental data presented in this paper can be used for this purpose.

Acknowledgements

Nomenclature

d_{10} = equivalent bubble diameter, (mm)
d_{32} = bubble Sauter diameter, (mm)
d_i = bubble diameter of the ith bubble class, (mm)
D = column diameter, (m)
j = mixture superficial velocity, (m/s)
m = exponent
n = exponent
n_i = number of bubbles in the ith bubble class
N = total number of bubbles

r = radial position, (m)
R = riser column radius, (m)
U = superficial velocity, (m/s)
v = velocity fluctuation, (m/s)
v' = average velocity fluctuation, (m/s)
V = linear velocity, (m/s)
z = height above gas sparger, (m)

Greek letter

α = local fractional gas hold-up

Subscripts

c = center of column
d = downcomer
G = gas
L = liquid
r = riser

References

Akita, K., T. Okazaki and H. Koyama, "Gas Holdups and Friction Factors of Gas–Liquid Two-Phase Flow in an Air-lift Bubble Column", J. Chem. Eng. Japan **21**, 476–482 (1988).

Becker, S., A. Sokolichin and G. Eigenberger, "Gas–Liquid Flow in Bubble Columns and Loop Reactors: Part II. Comparison of Detailed Experiments and Flow Simulations", Chem. Eng. Sci. **49**, 5747–5762 (1994).

Bentifraouine, C., "Hydrodynamique globale, locale et transfert de matière dans un réacteur airlift à boucle externe", Doctoral Thesis, ENSIGC, INP Toulouse, France (1997).

Bentifraouine, C., C. Xuereb and J.-P. Riba, "An Experimental Study of the Hydrodynamic Characteristics of External Loop Airlift Contactors", J. Chem. Tech. Biotech. **69**, 345–349 (1997).

Bruun, H. H., "Hot-wire Anemometry. Principles and Signal Analysis", Oxford University Press, Oxford (1995).

Calderbank, P. H., "Mass Transfer in Fermentation Equipment", in "Biochemical and Biological Engineering Science", vol. 1, N. Blakebrough, Ed., Academic Press, London, UK (1967), pp. 101–180.

Chisti, M. Y., B. Halard and M. Moo-Young, "Liquid Circulation in Airlift Reactors", Chem. Eng. Sci. **43**, 451–457 (1988).

Chisti, M. Y., "Airlift Bioreactors", Elsevier Applied Science, New York, NY (1989).

Choi, K. H. and W. K. Lee, "Comparison of Probe Methods for Measurement of Bubble Properties", Chem. Eng. Commun. **91**, 35–47 (1990).

Clark, N. N. and R. Turton, "Chord Length Distributions Related to Bubble Size Distributions in Multiphase Flows", Int. J. Multphase Flow **14**, 413–424 (1988).

Garcia Calvo, E., "Fluid Dynamics of Airlift Reactors: Two-Phase Friction Factors", AIChE J. **38**, 1662–1666 (1992).

Garcia Calvo, E. and P. Letón, "A Fluid Dynamic Model for Bubble Columns and Airlift Reactors", Chem. Eng Sci. **46**, 2947–2951 (1991).

Garcia Calvo, E. and P. Letón, "Prediction of Gas Hold-Up and Liquid Velocity in Airlift Reactors Using Two-Phase Flow Friction Coefficients", J. Chem. Tech. Biotech. **67**, 388–396 (1996).

Hsu, Y. C. and M. P. Dudukovic, "Gas Holdup and Liquid Recirculation in Gas-Lift Reactors", Chem. Eng. Sci. **35**, 135–141 (1980).

Hyndman, C. L., F. Larachi and C. Guy, "Understanding Gas-Phase Hydrodynamics in Bubble Columns: a Convective Model Based on Kinetic Theory", Chem. Eng. Sci. **52**, 63–77 (1997).

Kamp, A. M., C. Colin and J. Fabre, "Techniques de mesure par sonde optique double en écoulement diphasique à bulles", Cert Onéra, Colloque de Mécanique des Fluides Expérimentale, Toulouse, France, May 11-12 (1995).

Liu, T. J., "Bubble Size and Entrance Length Effects on Void Development in a Vertical Channel", Int. J. Multiphase Flow **19**, 99–113 (1993).

Liu, T. J. and S. G. Bankoff, "Structure of Air-Water Bubbly Flow in a Vertical Pipe – I. Liquid Mean Velocity and Turbulence Measurements", Int. J. Heat Mass Trans. **36**, 1049–1060 (1993).

Lübbert A. and B. Larson, "Detailed Investigations of the Multiphase Flow in Airlift Tower Loop Reactors", Chem. Eng. Sci. **45**, 3047–3053 (1990).

Marks, C. H., "Measurements of the Terminal Velocity of Bubbles Rising in a Chain, J. Fluids. Eng. **95**, 17–22 (1973).

Menzel T., T. in der Weide, O. Staudacher, O. Wein and U. Onken, "Reynolds Shear Stress for Modeling of Bubble Column Reactors", Ind. Eng. Chem. Res. **29**, 988–994 (1990).

Merchuk, J. C., N. Ladwa, A. Cameron, M. Bulmer and A. Pickett, "Concentric-Tube Airlift Reactors: Effects of Geometrical Design on Performance", AIChE J. **40**, 1105–1900 (1994).

Nicol, R. S. and J. F. Davidson, "Gas Hold-up in Circulating Bubble Columns", Chem. Eng. Res. Des. **66**, 152–158 (1988).

Roig, V., C. Suzanne and L. Masbernat, "Experimental Investigation of a Turbulent Bubbly Mixing Layer", Int. J. Multiphase Flow **24**, 35–54 (1998).

Rueffer, H. M., S. Broering, and K. Schuegerl, "Fluiddynamic Characterization of Airlift Tower Loop Bioreactors with and without Motionless Mixers", Bioprocess Eng. **12**, 119–130 (1995).

Russell, A. B., C. R. Thomas and M. D. Lilly, "The Influence of Vessel Height and Top-Section Size on the Hydrodynamic Characteristics of Airlift Fermentors", Biotech. Bioeng. **43**, 69–76 (1994).

Schmidt, J., R. Nassar and A. Lübbert, "Influence of the Wakes in Bubble Driven Multiphase Flow Systems", Chem. Eng. Sci. **47**, 2295–2300 (1992).

Siegel, M. and J. C. Merchuk, "Hydrodynamics in Rectangular Airlift Reactors: Scale-up and the Influence of Gas–Liquid Separator Design", Can. J. Chem. Eng. **69**, 465–473 (1991).

Sokolichin, A. and G. Eigenberger, "Gas–Liquid Flow in Bubble Columns and Loop Reactors: Part I. Detailed Modelling and Numerical Simulation", Chem. Eng. Sci. **49**, 5735–5746 (1994).

Utiger, M., "Étude de l'hydrodynamique locale d'un réacteur air-lift à boucle externe par anémométrie à film chaud", M.Sc.A. Thesis, École Polytechnique de Montréal, QC, Canada (1998).

Young, M. A., R. G. Carbonell and D. F. Ollis, "Airlift Bioreactors: Analysis of Local Two-Phase Hydrodynamics", AIChE J. **37**, 403–428 (1991).